THE JOURNAL OF BIOLOGICAL CHEMISTRY VOL. 288, NO. 51, pp. 36648–36661, December 20, 2013

The p38-interacting Protein (p38IP) Regulates G_2/M Progression by Promoting α-Tubulin Acetylation via Inhibiting Ubiquitination-induced Degradation of the Acetyltransferase GCN5*

Received for publication, May 21, 2013, and in revised form, November 11, 2013 Published, JBC Papers in Press, November 12, 2013, DOI 10.1074/jbc.M113.486910

Xin Liu[‡], Wei Xiao[‡], Xu-Dong Wang[‡], Yue-Fang Li[‡], Jiahuai Han[§], and Yingqiu Li[‡1]

From the [‡]Key Laboratory of Gene Engineering of the Ministry of Education, State Key Laboratory of Biocontrol, School of Life Sciences, Sun Yat-sen University, Guangzhou 510275 and the [§]State Key Laboratory of Cellular Stress Biology, School of Life Sciences, Xiamen University, Xiamen 361005, China

Background: The role of p38IP in cell cycle regulation remains unclear.
Results: p38IP inhibits ubiquitination-induced GCN5 degradation and therefore promotes α-tubulin acetylation, facilitating spindle formation and G_2/M progression.
Conclusion: p38IP is required for G_2/M progression.
Significance: This study reveals the necessity of p38IP for GCN5 stability and for G_2/M progression.

p38-interacting protein (p38IP) is a component of the GCN5 histone acetyltransferase-containing coactivator complex (GCN5-SAGA complex). It remains unclear whether p38IP or GCN5-SAGA is involved in cell cycle regulation. Using RNA interference to knock down p38IP, we observed that cells were arrested at the G_2/M phase, exhibiting accumulation of cyclins, shrunken spindles, and hypoacetylation of α-tubulin. Further analysis revealed that knockdown of p38IP led to proteasome-dependent degradation of GCN5. GCN5 associated with and acetylated α-tubulin, and recovering GCN5 protein levels in p38IP knockdown cells by ectopic expression of GCN5 efficiently reversed α-tubulin hypoacetylation and G_2/M arrest. During the G_2/M transition, the association of α-tubulin with GCN5 increased, and the acetylation of α-tubulin reached a peak. Biochemical analyses demonstrated that the interaction between p38IP and GCN5 depended on the p38IP N terminus (1–381 amino acids) and GCN5 histone acetyltransferase domain and bromodomain. The p38IP N terminus could effectively reverse p38IP depletion-induced GCN5 degradation, thus recovering α-tubulin acetylation and G_2/M progression. p38IP-mediated suppression of GCN5 ubiquitination most likely occurs via nuclear sequestration of GCN5. Our data indicate that the GCN5-SAGA complex is required for G_2/M progression, mainly because p38IP promotes the acetylation of α-tubulin by preventing the degradation of GCN5, in turn facilitating the formation of the mitotic spindle.

GCN5 (general control non-derepressible 5) is named for its original role in yeast general control of the amino acid synthesis pathway, and yeast strains with GCN mutations cannot derepress a number of amino acid biosynthetic genes during amino acid starvation (1, 2). Later, GCN5 was proved to be a transcription-related histone acetyltransferase (HAT)[2] (3, 4). GCN5 displays a sequence structure and enzyme specificity that are highly evolutionarily conserved from yeast to humans (5, 6). In addition to its roles in transcriptional modulation, the potential functions of GCN5 in cell cycle regulation have also been identified in yeast and in mammalian cells. In yeast, the absence of GCN5 induced several types of mitotic abnormalities, including cell cycle G_2/M arrest, chromosome loss, and defects in spindle elongation (7, 8). During mammalian embryogenesis, disruption of GCN5 was lethal due to increased cell apoptosis and G_2/M retardation (9–11).

In yeast cells, GCN5 was found to coexist with Ada2 (adaptor protein for transcriptional activation) in a multiprotein complex in 1994 (12); this complex was characterized and named as SAGA (Spt-Ada-GCN5 acetyltransferase)[3] with GCN5 as its catalytic core after several years of research in yeast (13, 14). In mammalian cells, there are two evolutionarily diverged GCN5 acetylase complexes: SAGA and ATAC (Ada2a or Ada Two-A-containing); both have their own specific subunits while they share a common GCN5 catalytic subunit (14). These complexes have essential but distinct functions in transcription, histone modification, signaling pathways, and cell cycle regulation (14).

p38IP (p38 mitogen-activated protein kinase-interacting protein) was first identified in a search for p38 binding partners using the yeast two-hybrid system (National Center for Biotechnology Information (NCBI) accession number AF093250). p38IP is required for the down-regulation of E-cadherin during mouse gastrulation via its activation of p38 (15). Using mass

* This work was supported by the Ministry of Science and Technology of China (Grants 2009CB522200 and 2013CB835300) and the National Natural Science Foundation of China (Grant 31170846).

[1] To whom correspondence should be addressed: State Key Laboratory of Biocontrol, Key Laboratory of Gene Engineering of the Ministry of Education, School of Life Sciences, Sun Yat-sen University, No. 135, Xingang Xi Road, Guangzhou 510275, China. Tel.: 86-20-39332848; Fax: 86-20-39332848; E-mail: lsslyq@mail.sysu.edu.cn.

[2] The abbreviations used are: HAT, histone acetyltransferase; ATAC, Ada2a or Ada Two-A-containing; ySpt20, yeast Spt20; BD, bromodomain deleted; p38IP, p38-interacting protein; WCL, whole cell extracts.

[3] Spt proteins (named for suppressor of TTy (SPT) genes) can restore gene expression disrupted by the insertion of the Ty transposable element in the yeast *Saccharomyces cerevisiae* (39).

spectrometry, p38IP was identified as a novel specific subunit of the human GCN5-SAGA and is highly similar to yeast Spt20 (ySpt20), which is a subunit of yeast SAGA (ySAGA) (16, 17). Human p38IP also exhibits similar regulatory functions to ySpt20 in the regulation of SAGA complex assembly and endoplasmic reticulum stress-induced genes (13, 16, 18). Recently, p38IP has been discovered to participate in starvation-induced autophagy via its regulation of mammalian Atg9 trafficking (19). These results suggest that p38IP is a multifunctional protein. However, so far, studies on p38IP are very limited, and it is unclear whether p38IP is involved in cell cycle regulation.

Recently, upon the ablation of its specific subunit Ada2a, the ATAC-GCN5 complex has been proven to be essential for cell cycle mitotic progression; by contrast, disruption of SAGA complex by knockdown of p38IP, a specific subunit of the GCN5-SAGA complex, did not lead to a cell cycle defect (20). This study suggests that the ATAC complex endows GCN5 with its role in the G_2/M transition, but ruled out the possibility of regulatory functions of p38IP as well as SAGA complex in the cell cycle progression (14, 20). In other words, p38IP may obstruct GCN5 regulation of the cell cycle progression.

In this study, we demonstrated that p38IP plays an essential role in G_2/M progression. In the absence of p38IP, cells showed a retardation of the G_2/M phase progression, abnormal spindle formation, and a hypoacetylation of α-tubulin. We discovered that p38IP maintained GCN5 stability by suppressing ubiquitination-induced degradation of GCN5. GCN5 associated with α-tubulin independent of p38IP. During G_2/M progression, the association of GCN5 with α-tubulin increased, thus promoting acetylation of α-tubulin and facilitating G_2/M progression. The N terminus (1–381 amino acids) of p38IP was identified as the key domain for interacting with and inhibiting the ubiquitination of GCN5, and correspondingly the p38IP N terminus could promote the nuclear translocation of cytosolic GCN5 HAT&BD truncated construct, whereas knockdown of p38IP increased the ratio of cytosolic to nuclear localization of GCN5, suggesting that p38IP may stabilize GCN5 via nuclear sequestration of GCN5. Our results demonstrate the essential roles and underlying mechanism of p38IP and the GCN5-SAGA complex in cell cycle regulation.

MATERIALS AND METHODS

Plasmids and siRNAs—p38IP was amplified from HeLa cDNA and introduced into the pYFP-C1 and pCMV5-HA vectors using the EcoRI and BamHI restriction sites. p38IP-N (1–381 amino acids) and p38IP-C (380–733 amino acids) were cloned into pEYFP-C1 using EcoRI and BamHI restriction sites. GCN5 was amplified by PCR from the cDNA of HeLa cells and cloned into the EcoRI and KpnI restriction sites of pFlag-CMV2 (Sigma). GCN5ΔBD, GCN5ΔHAT&BD, and GCN5HAT&BD were also cloned into pFlag-CMV2 using the same sites. The scrambled control short hairpin RNA (shRNA) (5′-CGCTAATTCGACTCGGATA-3′) and the p38IP mRNA-specific (shp38IP) (NM_001014286) shRNAs (shp38IP-1, target sequences, 5′-GCTTGTTATGCAAGAGACT-3′, ORF, and shp38IP-2, target sequences, 5′-ACACAAGAGCACTGAATCA-3′, 3′-UTR) were inserted into the RNA interference expression vector pSUPER.Retro.Neo-GFP (OligoEngine, Seattle, WA) for RNAi expression in cells. siRNA duplexes targeting human p38IP (sip38IP-1, 5′-CAAACAGACUGCUCUAUAAdTdT-3′, ORF), (sip38IP-2, 5′-GCUUGUUAUGCAAGAGACUdTdT-3′, ORF), and GCN5 (siGCN5, 5′-GGAAAUGCAUCCUGCAGAUdTdT-3′) were obtained from RiboBio Co. Ltd (Guangzhou, China).

Reagents and Antibodies—Thymidine and nocodazole were purchased from Sigma. Cycloheximide and MG132 were from Calbiochem. α-Tubulin (T5168) and FLAG (M2) were from Sigma; anti-acetyl-α-tubulin (ab24610) was from Abcam (Cambridge, MA); HA (12CA5) was from Roche Applied Science; GCN5 (C26A10) (3305) was from Cell Signaling Technology (Beverly, MA); and actin (5A7) was from Abmart (Shanghai, China). HA-probe (Y-11) (sc-805), GCN5 (N-18) (sc-6303), FAM48A (P-16) (sc-84118), FAM48A (S-19) (sc-84119), actin (I-19) (sc-1616), lamin B (M-20), cyclin A (H-432) (sc-751), cyclin B1 (GNS1) (sc-245), GFP (B-2) (sc-9996), ubiquitin (P4D1) (sc-8017), and HRP-conjugated secondary antibodies were purchased from Santa Cruz Biotechnology (Santa Cruz, CA). Alexa Fluor 488-, Alexa Fluor 594-, and Alexa Fluor 647-labeled secondary antibodies were from Molecular Probes (Eugene, OR). As GFP (B-2) is also reactive against YFP, it was used for detection of YFP.

Cell Culture, Transfections, and Synchronization—HeLa, MCF-7, MDA-MB-231, and 293T cells were grown in Dulbecco's modified Eagle's medium (Invitrogen) supplemented with 10% (v/v) fetal bovine serum (HyClone, Logan, UT), 100 units/ml streptomycin, and 100 units/ml penicillin (Invitrogen) at 37 °C, 5% CO_2. shp38IP HeLa cells, which were transfected with short hairpin RNA against p38IP and sorted for GFP fluorescence after 24 h, were cultured in the above conditions with the addition of 0.5 mg/ml G418 and were maintained for a few generations. Transient transfection of HeLa and 293T cells was carried out using TurboFect transfection reagent (Thermo Fisher Scientific) and Lipofectamine 2000 (Invitrogen), respectively, according to the manufacturer's protocol. For synchronization at G_1/S, HeLa cells were incubated with 2 mM thymidine for 18 h, released into thymidine-free medium for 9 h, then recultured in the presence of 2 mM thymidine for another 17 h. S, G_2, and M phase cells were harvested sequentially at 4, 8, and 10 h after release from thymidine block. MCF-7 cells were incubated for 24 h in culture with 2 mM thymidine for G_1/S synchronization. For G_2/M arrest, cells were treated with nocodazole (100 ng/ml) for 16 h.

Cell Proliferation Assay and Flow Cytometric Analysis—Equal numbers of control and p38IP-deficient cells were seeded and harvested at the indicated time points. Cell number was calculated by using a Z1 single threshold particle counter (Beckman Coulter). For flow cytometric analysis, cells were trypsinized, fixed overnight in 70% ice-cold ethanol, and then washed with PBS, incubated in RNase (100 μg/ml) for 10 min, stained with propidium iodide (50 μg/ml) for 1 h at room temperature, and analyzed with a FACSCalibur (BD Biosciences) using CellQuest software. ModFit and FlowJo software were used for data analysis.

Real-time PCR—Total RNA was extracted from HeLa cells using TRIzol reagent (Invitrogen) and reverse-transcribed into cDNAs followed by real-time PCR (quantitative PCR) using

SYBR Green (Roche Applied Science). Relative quantitative RNA was normalized with the housekeeping gene GAPDH. Primer sequences used for the reactions were as follows: GCN5 (sense, 5′-CTGAAGACCATGACTGAGCGG-3′, antisense, 5′-TCGGCCACAAAGAGCTTCC-3′), GAPDH (sense, 5′-ACGGATTTGGTCGTATTGGG-3′, antisense, 5′-TGATTTTGGAGGGATCTCGC-3′).

Western Blotting and Immunoprecipitation—Monolayer cells were harvested with lysis buffer (20 mM Tris-HCl, pH 7.5, 150 mM NaCl, 5 mM EDTA, pH 8.0, 5 mM $NaPP_i$, 1 mM sodium orthovanadate (Na_3VO_4), 1 mM PMSF, 1% Nonidet P-40, and 10 μg/ml aprotinin and leupeptin each). For ubiquitin samples, 0.1% SDS was added. After centrifugation at 15,000 $\times$ *g* to remove cell debris, the supernatant was denatured in 1×SDS loading buffer, boiled, and run on denaturing gels. Proteins were transferred onto PVDF membranes at 400 mA. After blocking in 4% BSA for 1 h, membranes were incubated in primary antibodies with 2% BSA overnight at 4 °C followed by HRP-conjugated secondary antibodies for 1 h at room temperature. For immunoprecipitations, after overnight incubation with the indicated antibodies, proteins were immunoprecipitated with protein G-Sepharose (GE Healthcare) for an additional 4 h at 4 °C. Immunoprecipitated beads were washed with lysis buffer at least three times, denatured by boiling in 2× SDS loading buffer, and subjected to SDS-PAGE.

Immunofluorescence—Cells were plated at 50∼70% densities on glass slides. At the indicated time points, cells were collected, fixed with 4% paraformaldehyde, and permeabilized with 0.2% Triton X-100. After blocking with 2% BSA for 1 h, cells were incubated in primary antibody overnight at 4 °C and then incubated in Alexa Fluor 488-, Alexa Fluor 594-, or Alexa Fluor 647-labeled secondary antibody for 1 h at room temperature, mounted in mounting medium, and analyzed by confocal microscopy (Leica Microsystems, Heidelberg GmbH, Leica SP5 microscope confocal). Laser excitations at 405, 488, 550, and 633 nm were used in the research. Spindle length was taken as the distance between two mitotic centrosomes; the spindle width was defined as the largest distance over which kinetochores spread out (21–23). For calculation of *z* distance between mitotic centrosomes, one centrosome was marked as Z1 followed by scanning along the *z* axis of the microscope at 0.2-μm increments until reaching the other centrosome (Z2), and thus the *z* distance is the vertical distance between two mitotic centrosomes, which were labeled by γ-tubul in (22). ImageJ software was used to quantify the ratio of cytosolic/nuclear GCN5 protein levels. Specifically, the total immunofluorescence intensity of GCN5 in the whole cell (WI) or in the nucleus (NI), as well as in areas of the cell (WA) or the nucleus (NA), were quantified separately, and then the cytosol area-average fluorescence intensity (C) was obtained by the formula (WI − NI)/(WA − NA), whereas the nucleus area-average fluorescence intensity (N) was obtained by the formula NI/NA. Finally the ratio C/N was obtained to present the area-average fluorescence intensity ratio of cytosolic GCN5 to nuclear GCN5.

Nuclear Extraction—Cells were washed twice with ice-cold PBS supplemented with 1 mM EDTA and resuspended in five packed-cell volumes of cytosolic extraction buffer (10 mM Hepes-KOH (pH 7.9), 60 mM KCl, 1 mM EDTA, 0.54% Nonidet P-40, 1 mM DTT, 1 mM PMSF, and 10 μg/ml aprotinin and leupeptin each). After centrifugation at 4,000 $\times$ *g* for 5 min, pelleted nuclei were washed in cytosolic extraction buffer and then lysed with nuclear extraction buffer (250 mM Tris (pH 7.8), 60 mM KCl, 1 mM EDTA, 1 mM DTT, 1 mM PMSF, and 10 μg/ml aprotinin and leupeptin each) for 10 min at 4 °C. After freezing and thawing three times, nuclear extracts were pelleted by centrifugation at 14,000 $\times$ *g*.

Statistical Analysis—All experiments presented were repeated at least three times. Statistical analysis was performed using Student's *t* test (GraphPad Prism V5.0; GraphPad Software).

RESULTS

Depletion of p38IP Impairs Cell Proliferation and Induces a Defective Cell Cycle—ySpt20, the homologue of p38IP in yeast, regulates yeast cell proliferation by stabilizing the integrity of the SAGA complex; however, the detailed mechanism underlying this phenomenon is still unclear. Furthermore, whether p38IP exhibits an evolutionarily conserved function in the modulation of mammalian cell proliferation has not been shown. If so, how it participates in this process remains unknown. To address these questions, we checked the cell proliferation rate after knockdown of p38IP. HeLa cells expressing p38IP-specific short hairpin RNAs showed remarkably impaired cell proliferation (Fig. 1*A*) (shp38IP-1 and shp38IP-2, targeting the reading frame and the 3′-UTR of p38IP, respectively; shp38IP-1 was used in the following experiments and is referred to as shp38IP). Depletion of p38IP in MCF-7 or MDA-MB-231 cells using specific small interfering RNAs (sip38IP-1 and sip38IP-2, targeting different coding regions) also decreased cell proliferation (Fig. 1, *B* and *C*). To further understand this phenomenon, flow cytometric analysis was employed to examine cell cycle distribution. As shown in Fig. 1*D*, p38IP depletion resulted in a significant increase in the number of cells in G_2/M phase. After synchronization at the G_1/S boundary using a thymidine double block at the indicated time points after release, p38IP-depleted cells showed an obvious cell cycle arrest in G_2/M and a slight retardation at the G_1/S transition. It was found that HeLa control cells synchronously entered S phase at 4 h after release, whereas p38IP-deficient cells proceeded into S phase and a small percentage (∼5.8%) lagged in G_1 phase. At 10 h after release, ∼46% of the control cells and only 16% of the shp38IP cells underwent cell mitosis with 2N DNA content (Fig. 1*E*). Similar results were also observed in MCF-7 cells expressing the p38IP-specific short hairpin RNAs (Fig. 1*F*). These results indicate that p38IP is critical for cell cycle G_2/M progression. Because degradation of mitotic cyclins was closely correlated with cell cycle G_2/M progression (24–26), we further examined the protein levels of mitotic cyclins in shp38IP cells and found that the protein abundance of cyclin A and cyclin B was significantly enhanced after p38IP depletion (Fig. 1*G*). We synchronized the cells at G_1/S or G_2/M using thymidine or nocodazole, respectively. After the control cells were released from the G_1/S boundary, cyclin A exhibited an increase and then a subsequent decrease at 10 h and a disappearance at 12 h. By contrast, cyclin A levels were sustained at 12 h in p38IP-depleted cells (Fig. 1*H*). A similar pattern of cyclin

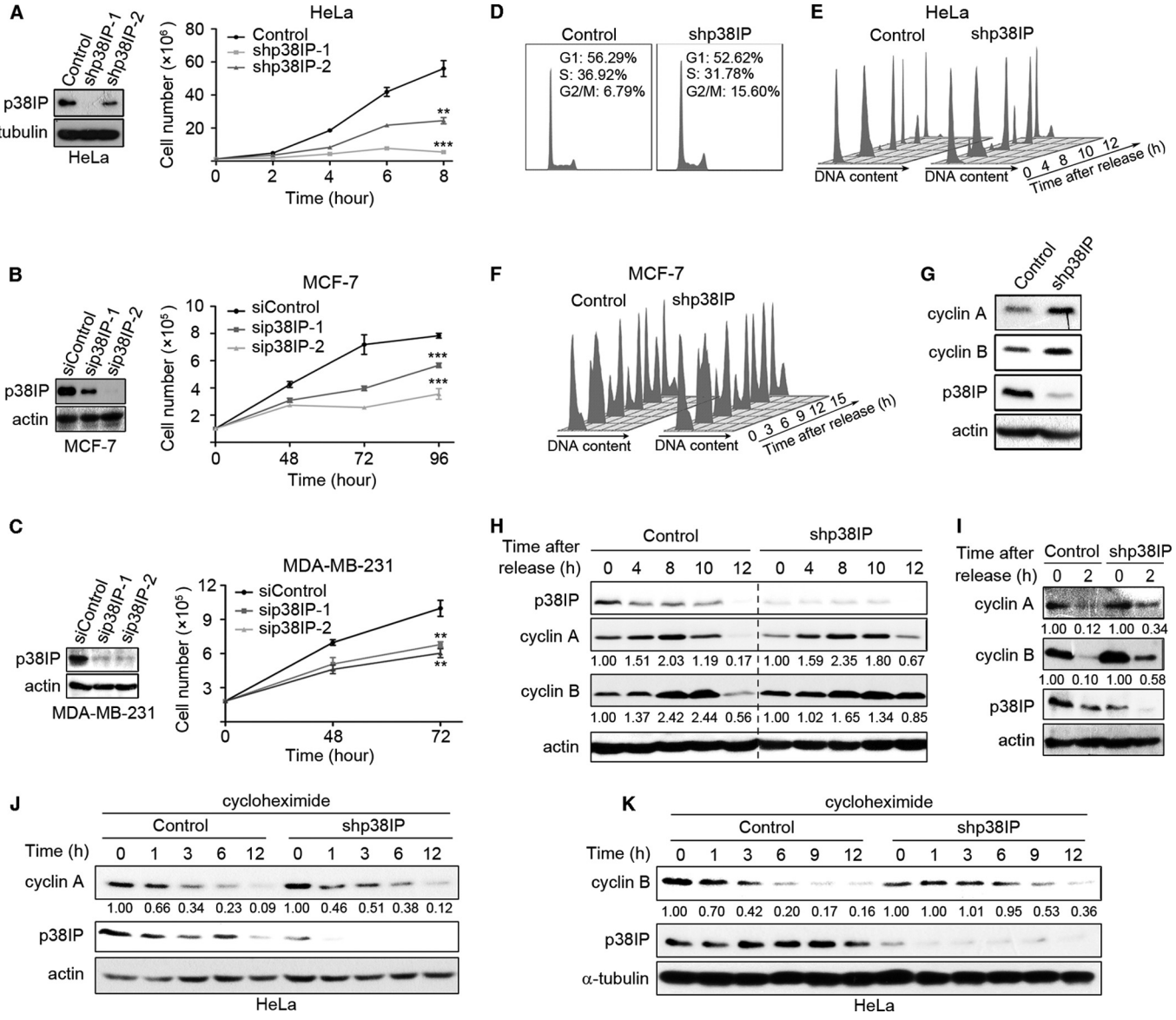

FIGURE 1. **Depletion of p38IP impairs cell proliferation and induces a defective cell cycle.** *A–C*, p38IP depletion impaired cell proliferation in HeLa, MCF-7, and MDA-MB-231 cells. *Left panel*: Western blot analysis of p38IP depletion efficiency in HeLa (*A*), MCF-7 (*B*), and MDA-MB-231 (*C*) cells. α-Tubulin or actin served as the loading control. *Right panel*: cell proliferation was measured at the indicated time points in control and p38IP-depleted cells as described under "Materials and Methods" (mean ± S.D., $n = 3$, **, $p < 0.05$, ***, $p < 0.001$). *D*, accumulated cells in G_2/M after p38IP depletion. Cell cycle distribution was analyzed using propidium iodide staining and flow cytometry in asynchronous HeLa cells. *x* axis: DNA content; *y* axis, cell numbers. The data presented were representative of three independent experiments. *E* and *F*, impaired cell cycle progression after p38IP depletion. HeLa (*E*) and MCF-7 (*F*) cells were synchronized using thymidine block and harvested at the indicated times after release. Cells were stained using propidium iodide followed by flow cytometry analysis. *x* axis, DNA content; *y* axis, cell numbers. The data shown were representative of four independent experiments. *G*, p38IP depletion increased the endogenous levels of cyclin A and cyclin B in asynchronous HeLa cells. Whole cell extracts (WCL) were prepared from asynchronous HeLa cells and analyzed using Western blot with the indicated antibodies. *H*, depletion of p38IP postponed the degradation of cyclin A and cyclin B in the cell cycle. Cell extracts were prepared from cells released from the G_1/S block at the indicated time points for immunoblotting with the indicated antibodies. The densitometric intensities of cyclin A and cyclin B blot signals were normalized to actin; the relative intensity value when compared with that of the starting point sample is shown below each panel. *I*, p38IP depletion caused the accumulation of cyclin A in the cell cycle. Cells were treated with nocodazole (100 ng/ml) for the G_2/M block. After release from the G_2/M boundary, cells were collected at the indicated time points and processed for immunoblotting. *J* and *K*, knockdown of p38IP postponed the degradation of cyclin A (*J*) and cyclin B (*K*). Cells were harvested at the indicated time points upon treatment of cycloheximide (40 μM) followed by Western blot analysis with the indicated antibodies.

B was also observed. Similarly, delayed degradation of cyclin A and B was also observed in shp38IP cells released from G_2/M phase (Fig. 1*I*). Analysis of the protein half-lives using cycloheximide showed that cyclin A and B had prolonged half-lives in p38IP-depleted cells (Fig. 1, *J* and *K*). Thus, the cell cycle-dependent degradation of cyclins was impaired.

p38IP Depletion Results in Defective Spindle Morphology—Interestingly, knockdown of p38IP resulted in a smaller cell size at metaphase (Fig. 2, *A* and *B*). In metaphase, most of the control cells were ~17–19 μm in diameter, whereas the majority of the p38IP-depleted cells exhibited a much smaller diameter between 14 and 16 μm (Fig. 2*C*). A similar phenomenon was observed in mitotic spindles. When compared with control cells, where the majority had approximate dimensions of 10–11 μm in length and no less than 7 μm in width, p38IP-deficient cells displayed a shrunken spindle shape, with the majority of

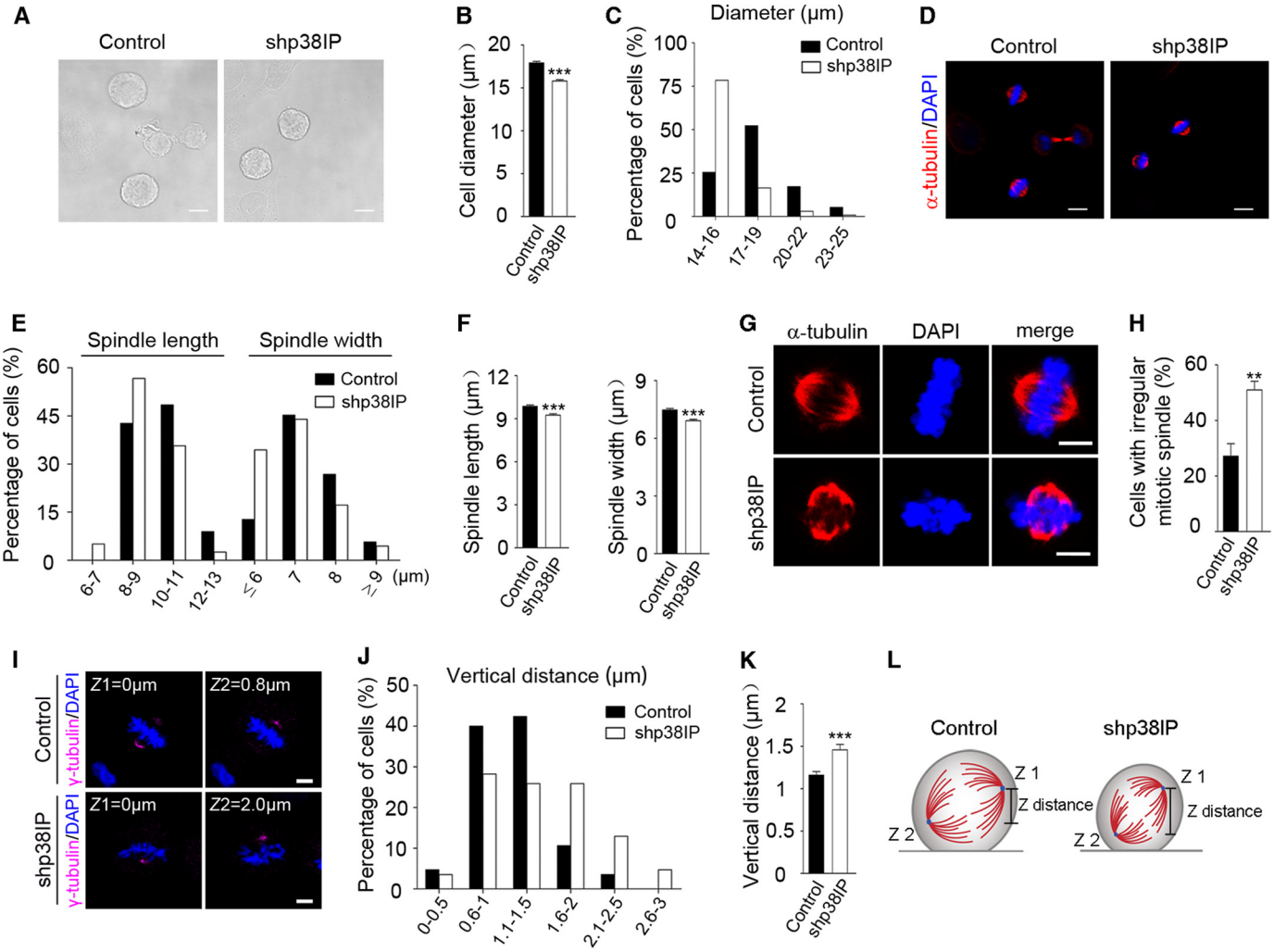

FIGURE 2. **p38IP depletion results in defective spindle morphology.** *A*, microscopic analysis of cell size in control and p38IP-depleted HeLa cells (*scale bar*: 10 μm). *B* and *C*, quantification of the average (*B*) and distribution (*C*) of the cell diameter in metaphase cells expressing shRNAs as indicated ($n = 135$ cells from three independent experiments, mean ± S.E., ***, $p < 0.001$). *D*, immunofluorescence analysis of the mitotic spindle in control and p38IP-depleted HeLa cells by staining with α-tubulin (*red*). DNA was visualized by 4,6-diamidino-2-phenylindole (DAPI, *blue*) (*scale bar*: 10 μm). *E*, distribution of spindle length and width in metaphase cells expressing shRNAs as indicated ($n = 155$ cells from three independent experiments). The spindle length and width were measured as described under "Materials and Methods." *F*, quantification of the average spindle length and width in cells expressing shRNAs as indicated ($n = 155$ cells from three independent experiments, mean ± S.E., ***, $p < 0.001$). *G*, immunofluorescence analysis of the mitotic spindle staining with α-tubulin antibody (microtubules, *red*) and DNA by DAPI (*blue*) (*scale bars*: 5 μm). *H*, quantification of cells with defective mitotic spindles in control and p38IP-depleted cells (50 cells/experiment, mean ± S.E., $n = 3$, **, $p < 0.05$). *I*, different *z* sections of cells stained for γ-tubulin (*purple*) in control and shp38IP HeLa cells. DNA was visualized by DAPI (*blue*) (*scale bar*: 5 μm). *J* and *K*, quantification of the distribution (*J*) and average (*K*) of the vertical distance between two centrosomes in metaphase cells expressing shRNAs as indicated ($n = 90$ cells from three independent experiments, mean ± S.E., ***, $p < 0.001$). *z* sections were taken at 0.2-μm increments as described under "Materials and Methods." *L*, a schematic representation of the *z* distance measurement in control and shp38IP cells.

the spindles being 8–9 μm in length and no more than 7 μm in width (Fig. 2, *D–F*). (Spindle length and width were measured as described under "Materials and Methods.") Moreover, the microscopic observation of α-tubulin revealed that knockdown of p38IP resulted in a high proportion of defective spindle formation, which was characterized by aberrant spindle fibers (Fig. 2*G*). The proportion of irregular spindles in the p38IP-deficient cells was approximately twice that of normal cells (Fig. 2*H*). Furthermore, centrosomal γ-tubulin was stained to indicate the spindle poles and the vertical or *z* distance (measured as described under "Materials and Methods") between the mitotic spindle poles and was measured in control and shp38IP cells. p38IP-deficient cells at metaphase tended to display an increased vertical distance between the two centrosomes. ~43.5% were greater than 1.5 μm and ~4.7% reached 2.6~3 μm, whereas only ~14.1% of the control cells were greater than 1.5 μm, and none reached 2.6–3 μm (Fig. 2, *I* and *J*); thus, the control and shp38IP cells had a significant difference in their vertical centrosome distances (Fig. 2*K*). Altogether, spindle assembly and orientation were both impaired upon p38IP depletion. A schematic of the control and p38IP-deficient cells at metaphase is shown in Fig. 2*L*.

Knockdown of p38IP Blocks α-Tubulin Acetylation—The mitotic spindle is a highly dynamic microtubule-based structure that consists of polymerized α/β-tubulin heterodimers. Acetylation of α-tubulin is closely related with microtubule stabilization, although the mechanism is still unclear (27–31). Thus, we wondered whether the shrunken spindle and G_2/M retardation induced by p38IP depletion may result from the abnormal acetylation of α-tubulin. As expected, depletion of

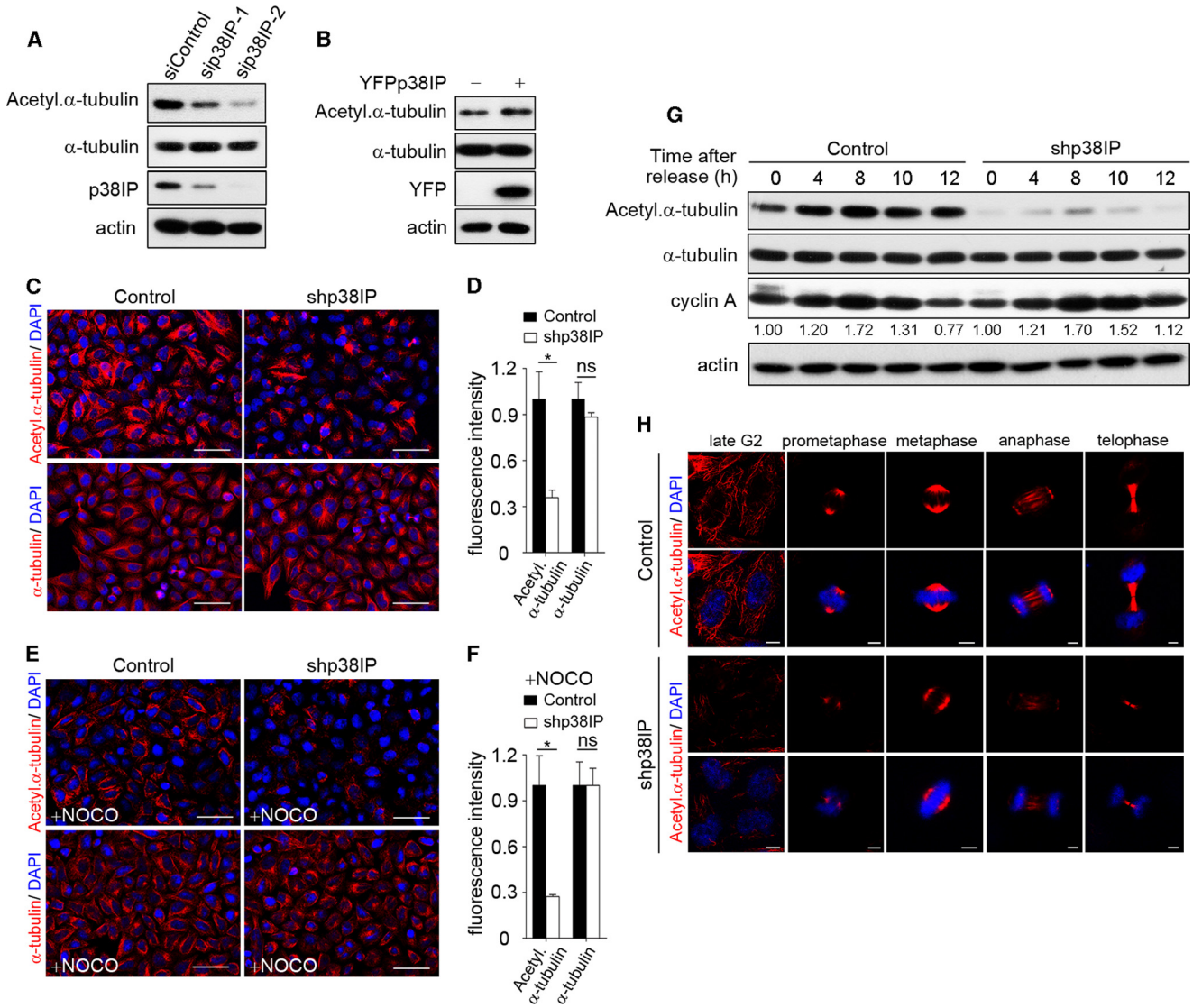

FIGURE 3. **Knockdown of p38IP blocks α-tubulin acetylation.** *A*, Western blot analysis of the cell lysates from HeLa cells expressing the indicated siRNAs using the specific antibodies. *B*, p38IP promoted the acetylation of α-tubulin. HeLa cells were transfected with YFP or YFP-p38IP. After 24 h, the cells were harvested for immunoblotting with the indicated antibodies. *C*, immunofluorescence was performed for acetylated α-tubulin (*red*) (*upper panels*) and α-tubulin (*red*) (*lower panels*) of control and p38IP-depleted cells. DNA was visualized by DAPI (*blue*) (*scale bars*: 50 μm). *D*, quantification of the average fluorescence intensity of acetyl-α-tubulin and α-tubulin in control and shp38IP cells (mean ± S.E., $n = 3$, *, $p < 0.05$, *ns* indicates no significant difference). *E*, cells were treated with 0.6 μM nocodazole for 20 min and collected for immunofluorescence analysis performed as that in *C* (*scale bars*: 50 μm). *F*, quantification of the average fluorescence intensity of acetyl-α-tubulin and α-tubulin in control and p38IP-depleted cells in the presence of nocodazole (mean ± S.E., $n = 3$, *, $p < 0.05$, *ns* indicates no significant deference). Three fluorescent microscopic fields were randomly selected in the control and shp38IP cells. The quantitative fluorescence intensity of acetyl-α-tubulin and α-tubulin in *D* and *F* were normalized by the acetyl-α-tubulin and α-tubulin fluorescence intensity in one of the selected microscopic fields in control cells. *G*, cell cycle distribution of acetylated α-tubulin in control and p38IP-depleted cells. After G_1/S synchronization by the thymidine double block, the cells were released at the indicated time points and collected for immunoblotting using the indicated antibodies. *H*, immunofluorescence analysis of acetylated α-tubulin in late G_2 and stages of cell mitosis. Control and p38IP-depleted HeLa cells in the indicated phases of cell cycle were fixed and stained with acetylated α-tubulin (*red*) and DAPI (*blue*) (*scale bar*: 5 μm).

p38IP using siRNAs targeting different sites of p38IP inhibited acetylation on lysine 40 of α-tubulin (Fig. 3*A*). Conversely, overexpression of p38IP promoted the acetylation of α-tubulin (Fig. 3*B*). We further confirmed these results by immunofluorescence analysis, which showed that shp38IP cells harbored a much weaker fluorescence intensity of acetylated α-tubulin when compared with control cells, whereas the overall fluorescence intensities of α-tubulin showed no difference (Fig. 3, *C* and *D*). Next, the cells were treated with the microtubule-depolymerizing agent nocodazole to disrupt highly dynamic microtubules. Microtubules in p38IP-depleted cells were more sensitive to nocodazole and crashed after 20 min of treatment, leading to a much weaker staining of acetylated α-tubulin (Fig. 3, *E* and *F*). These results indicate that the microtubules are unstable in the absence of p38IP. Furthermore, we compared the levels of acetylated α-tubulin at each step of the cell cycle in control and shp38IP cells after G_1/S synchronization. In control cells, the acetylation level of α-tubulin fluctuated throughout the cell cycle, increasing at 8 h (G_2/M) and decreasing at 12 h (G_1) after release; however, after depletion of p38IP, the levels of acetylated α-tubulin were maintained at a hypo-level during the entire cell cycle and demonstrated little elevation at the

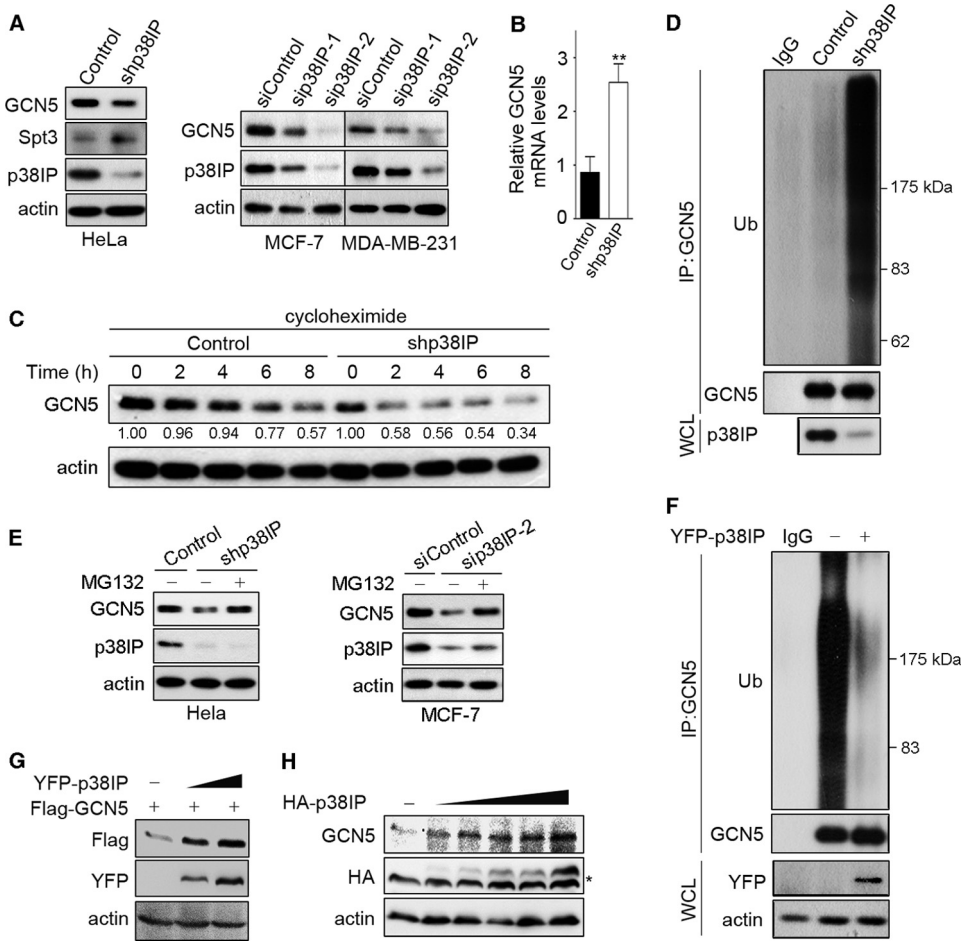

FIGURE 4. **p38IP maintains GCN5 stability.** *A*, GCN5 declined after p38IP knockdown. Cell extracts were prepared from HeLa cells expressing the indicated shRNAs or MCF-7 and MDA-MB-231 cells with the indicated siRNAs for Western blot analysis using specific antibodies. *B*, quantification of mRNA levels of GCN5 upon p38IP depletion. mRNA levels of GCN5 were examined using quantitative PCR. (mean ± S.D., $n = 3$, **, $p < 0.05$). *C*, p38IP depletion impaired GCN5 stability. Cells were harvested at the indicated time points upon 40 μM cycloheximide treatment and analyzed using Western blot analysis. *D*, disruption of p38IP resulted in the hyper-ubiquitination of GCN5 in HeLa cells. WCL were immunoprecipitated (*IP*) using the GCN5 antibody followed by immunoblotting with an anti-ubiquitin antibody. *Ub*, ubiquitin. *E*, MG132 stabilized GCN5 protein in p38IP-depleted cells. HeLa cells expressing the indicated shRNAs or MCF-7 transfected with p38IP siRNAs were treated with dimethyl sulfoxide (DMSO) or 10 μM MG132 for 4 h and then collected and processed for immunoblotting. *F*, p38IP decreased GCN5 ubiquitination. 293T cells transfected with or without YFP-p38IP were collected. Immunoprecipitation was then performed with anti-GCN5 followed by Western blot using an anti-ubiquitin antibody. *G* and *H*, p38IP increased the protein levels of GCN5. Protein extracts were prepared from 293T cells expressing FLAG-GCN5 with increasing concentrations of YFP-p38IP (*G*) or only expressing increasing doses of HA-p38IP (*H*) and blotted using the indicated antibodies. * indicates a nonspecific band.

G_2/M phase (Fig. 3*G*). Thus, p38IP may promote α-tubulin acetylation during the G_2/M phase, which is down-regulated after cell mitosis. Moreover, acetylated α-tubulin in late G_2 and each stage of cell mitosis was examined using immunofluorescence analysis. After p38IP depletion, the cells exhibited a much weaker acetylation of α-tubulin in the late G_2 phase, and the hypoacetylation of α-tubulin was sustained throughout mitosis (Fig. 3*H*). Taken together, all of these data suggest that p38IP serves as an important regulator of α-tubulin acetylation, which ensures the stability of microtubules for correct mitotic spindle conformation as well as for orderly cell cycle progression.

p38IP Maintains GCN5 Stability—Given that p38IP is important for the integrity of the SAGA complex and that GCN5, the catalytic subunit of the SAGA complex, serves as an acetyltransferase for α-tubulin in muscle cell differentiation (16, 29), we next analyzed GCN5 to determine whether it was related to p38IP depletion-caused defects in cell cycle progression and α-tubulin acetylation. We observed a remarkable reduction in GCN5 expression in p38IP-depleted cells (Fig. 4*A*). However, the abundance of Spt3, another subunit of the human SAGA complex, did not decrease after p38IP depletion. Increased mRNA levels of GCN5 indicated that down-regulation of GCN5 protein in shp38IP cells did not occur at the transcriptional level (Fig. 4*B*), and thus, the stability of GCN5 protein was confirmed. Upon cycloheximide treatment, GCN5 exhibited a much shorter half-life after p38IP depletion (Fig. 4*C*). Consistent with this finding, a robust elevation of ubiquitinated GCN5 was detected when p38IP was knocked down (Fig. 4*D*), and treatment with the proteasome inhibitor MG132 stabilized GCN5 protein in p38IP-depleted cells (Fig. 4*E*), indicating that p38IP depletion targets GCN5 for degradation via the ubiquitin-proteasome pathway. As expected, p38IP remarkably inhibited the ubiquitination of endogenous GCN5 (Fig. 4*F*), and the protein level of GCN5 was gradually increased

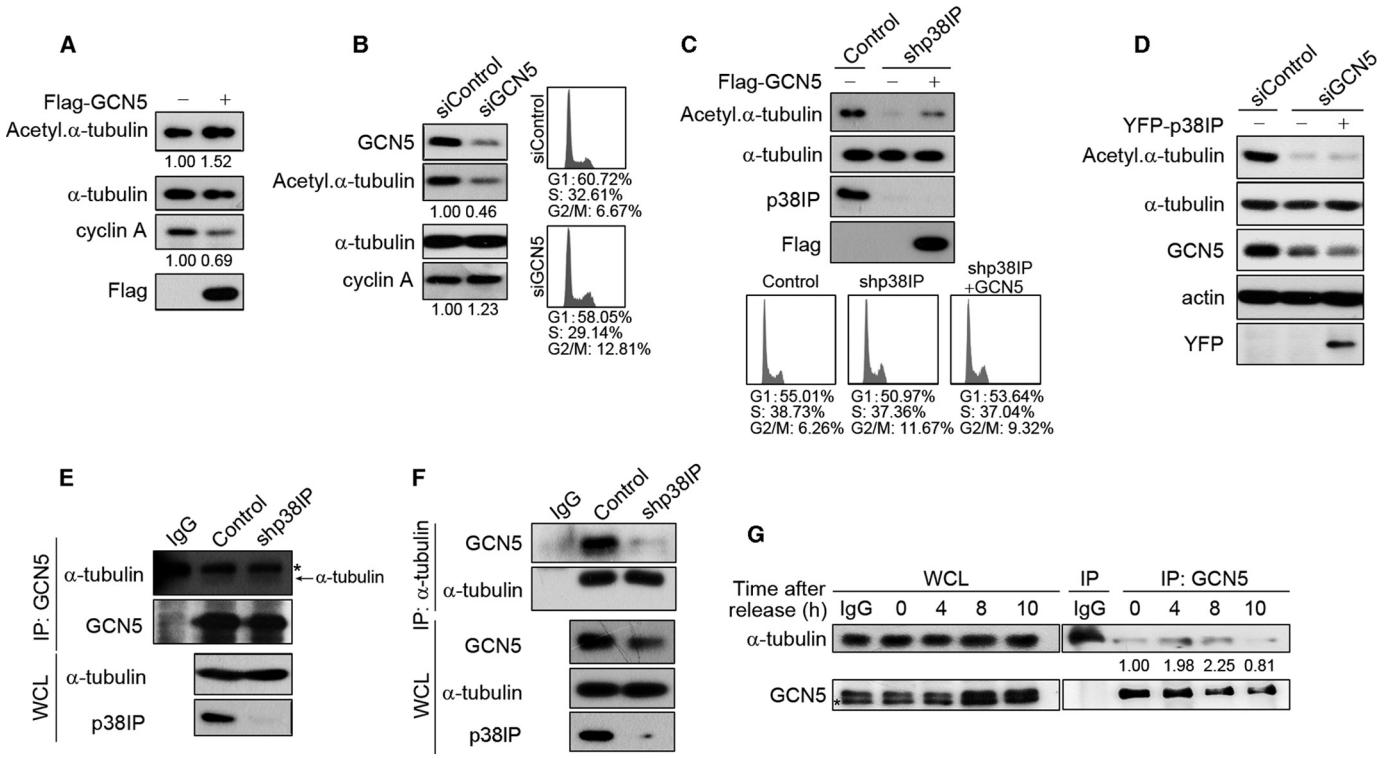

FIGURE 5. **GCN5 mediates p38IP depletion-induced α-tubulin hypoacetylation.** *A*, GCN5 enhanced α-tubulin acetylation. HeLa cells were transfected with FLAG-GCN5 or an empty vector and harvested 24 h later followed by immunoblotting with the indicated antibodies. *B*, GCN5 knockdown decreased the level of acetylated α-tubulin and cell G_2/M accumulation. HeLa cells were transfected with siControl or siRNA oligonucleotides against GCN5. After 48 h, the cells were collected and processed for Western blot and flow cytometric analysis. *C*, re-expression of GCN5 alleviated α-tubulin hypoacetylation and G_2/M arrest in p38IP-depleted cells. Control and p38IP-depleted cells were transfected with empty or GCN5-expressing vectors and collected for immunoblotting with the indicated antibodies and flow cytometric analysis. *D*, p38IP restoration failed to rescue the hypoacetylated α-tubulin caused by GCN5 depletion. Control and GCN5-depleted HeLa cells were transfected with YFP or YFP-p38IP. Cells were collected for immunoblotting with the indicated antibodies. *E* and *F*, the association between GCN5 and α-tubulin was unaffected by p38IP depletion. WCL were prepared from control and shp38IP HeLa cells and processed for the immunoprecipitation (*IP*) of α-tubulin (*E*) or GCN5 (*F*) with anti-GCN5 and anti-α-tubulin antibody, respectively. *G*, the interaction between GCN5 and α-tubulin throughout cell cycle progression. HeLa cells were synchronized at the G_1/S boundary and collected at the indicated times after release and then immunoprecipitated with IgG or anti-GCN5 antibody and blotted with anti-α-tubulin antibody. * indicates a nonspecific band.

with increasing doses of transfected p38IP (Fig. 4, *G* and *H*). Taken together, these results suggest that p38IP serves as a critical regulator for maintaining GCN5 protein stability and in turn the integrity of SAGA.

p38IP Regulates the Acetylation of α-Tubulin via GCN5—Although the decrease in GCN5 levels might explain the phenomenon of accumulation of mitotic cyclins in p38IP-deficient cells, consistent with previous reports that ATAC-GCN5 induced the degradation of cyclin A via acetylation (20, 26), the decrease in both GCN5 protein level and α-tubulin acetylation upon p38IP depletion obviously contradicts the observed increase in α-tubulin acetylation caused by ATAC-GCN5 destruction (20). To date, it remains unclear whether and how α-tubulin acetylation is regulated by GCN5 in cell cycle progression. Thus, we focused on determining the mechanism of p38IP-GCN5 regulation on the acetylation of α-tubulin. First, we confirmed that GCN5 acetylates α-tubulin in HeLa cells. Overexpression and depletion of GCN5 promoted and inhibited the acetylation of α-tubulin and decreased and enhanced cyclin A, respectively, as expected (Fig. 5*A*). In addition, GCN5 depletion also caused cell cycle G_2/M arrest similar to p38IP depletion (Fig. 5*B*). We further restored GCN5 in p38IP-depleted cells and observed that re-expression of GCN5 relieved to some degree the hypoacetylation of α-tubulin as well as G_2/M arrest induced by p38IP depletion (Fig. 5*C*). By contrast, once GCN5 was depleted, re-expression of p38IP failed to reverse the siGCN5-induced hypoacetylation of α-tubulin (Fig. 5*D*). Moreover, GCN5 was constitutively associated with α-tubulin before and after p38IP depletion, ruling out the possibility that p38IP affected the interaction between GCN5 and α-tubulin (Fig. 5*E*); nevertheless, p38IP depletion-induced degradation of GCN5 resulted in little GCN5 binding to α-tubulin (Fig. 5*F*). The interaction between GCN5 and α-tubulin fluctuated through the cell cycle and increased at G_2/M transition (Fig. 5*G*), which coincided with the variation of acetylated α-tubulin through the cell cycle (Fig. 3*G*). Taken together, these results indicate that GCN5 may directly acetylate α-tubulin and that p38IP regulates the acetylation of α-tubulin via GCN5.

The N Terminus of p38IP Mediates Its Association with GCN5—To determine how p38IP regulates the stability of GCN5, we first identified the binding domains of p38IP and GCN5. p38IP was truncated into N- (amino acids 1–381) and C- (amino acids 380–733) terminal fragments as described previously (15) and then checked for association with GCN5. We found that full-length p38IP and the p38IP N terminus both bound to GCN5, whereas the p38IP C terminus failed to bind despite high expression (Fig. 6*A*). Next, the truncated proteins containing either amino acids 1–729 (GCN5ΔBD, bromodo-

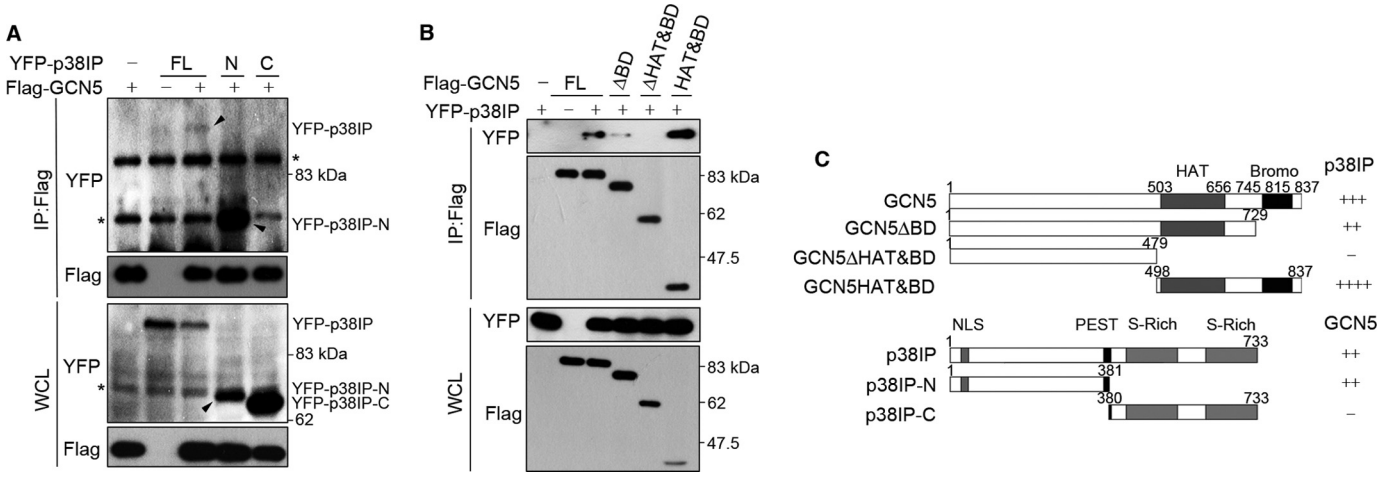

FIGURE 6. **The N terminus of p38IP mediates its association with GCN5.** *A*, cell extracts from 293T cells transfected with the indicated constructs were immunoprecipitated (*IP*) with anti-FLAG antibody followed by anti-YFP antibody immunoblotting. * indicates a nonspecific band. *FL*, full length; *N*, p38IP N terminus; *C*, p38IP C terminus. *B*, GCN5 associated with p38IP via HAT&BD domains. 293T cells transfected with the indicated plasmids were harvested, and lysates were immunoprecipitated with anti-FLAG antibody followed by anti-YFP antibody immunoblotting. *C*, schematic of interaction mapping of p38IP and GCN5. *GCN5ΔBD*, deleted bromodomain; *GCN5ΔHAT&BD*, deleted both HAT domain and bromodomain; *GCN5HAT&BD*, HAT domain and bromodomain.

main deleted),[4] 1–497 (GCN5ΔHAT&BD, both HAT domain and bromodomain deleted), or 498–837 (GCN5HAT&BD, HAT domain and bromodomain) were coimmunoprecipitated with YFP-p38IP (32). As shown in Fig. 6*B*, GCN5HAT&BD exhibited the strongest association with p38IP among the three mutants, whereas GCN5ΔBD only pulled down a trace amount of p38IP and GCN5ΔHAT&BD did not bind to p38IP at all. These results clearly indicate that the HAT domain and bromodomain of GCN5 and the N terminus of p38IP mediate their mutual interaction. The binding schematic diagram is shown in Fig. 6*C*.

The N Terminus of p38IP and the HAT Domain and Bromodomain of GCN5 Are Responsible for GCN5 Stability—Given that amino acids 1–381 in p38IP mediate its association with GCN5, we deduced that p38IP may regulate GCN5 stability via this region. As shown in Fig. 7, *A* and *B*, p38IP-N as well as full-length p38IP markedly increased GCN5 protein level by more than ~1.5-fold in contrast to p38IP-C, which had no effect on GCN5 abundance although it was highly expressed. Consistent with this result, the ubiquitination of GCN5 was also strikingly inhibited in the presence of p38IP-N and p38IP but not with p38IP-C (Fig. 7*C*). Next, we determined the domain of GCN5 conjugated with polyubiquitin chains. The results showed that GCN5HAT&BD was heavily ubiquitinated, whereas GCN5ΔHAT&BD was only slightly ubiquitinated (Fig. 7*D*), which is consistent with a previous study (33). We further observed that ubiquitination of GCN5HAT&BD was inhibited effectively by p38IP-N (Fig. 7*E*), demonstrating that their interaction is required for p38IP inhibition of GCN5 ubiquitination. Taken together, these results demonstrate that the N terminus of p38IP maintains the stability of GCN5 via association with GCN5 HAT&BD domain and in turn suppresses the ubiquitination of the HAT&BD domain.

[4] Bromodomain was first reported in and had its name from the *Drosophila* protein brahma. It is recognized as an acetyl-lysine binding domain evolutionarily conserved in many chromatin-associated proteins and nuclear histone acetyltransferase (40).

P38IP Promotes GCN5 Nuclear Translocation—Next, we explored how the interaction between p38IP and GCN5 blocks the ubiquitination of GCN5. Cytosolic localization of GCN5HAT&BD and nuclear localization of GCN5 and the ΔHAT&BD mutant were observed (Fig. 8*A*). We also observed the nuclear localization of both full-length p38IP and p38IP-N and the cytosolic localization of p38IP-C in 293T cells (Fig. 8*B*). Considering that GCN5HAT&BD was heavily ubiquitinated and mediated association with p38IP, we presumed that p38IP may stabilize GCN5 by promoting GCN5 nuclear translocation via its interaction. Therefore, we co-transfected GCN5HAT&BD with p38IP or p38IP-N. As expected, obvious GCN5HAT&BD nuclear translocation was detected (Fig. 8*C*). These results were further confirmed by cell fractionation experiments (Fig. 8, *D* and *E*). Next, GCN5 cellular localization after p38IP depletion was detected. By quantification of the area-average fluorescence intensities of GCN5 in the cytosol and nucleus, we found an increased ratio of cytosolic to nuclear GCN5 in the absence of p38IP (Fig. 8, *F* and *G*). (The measurement of area average fluorescence intensities of GCN5 is described under "Materials and Methods.") To confirm this result and to avoid the degradation of cytosolic GCN5, further cell fractionation assays were performed in the presence of MG132. Consistently, p38IP depletion led to increased cytosolic GCN5 and decreased nuclear GCN5 (Fig. 8*H*). These results indicate that upon p38IP depletion, GCN5 has a higher cytosolic localization. Taken together, these observations suggest that p38IP may stabilize GCN5 by retaining it in the nucleus.

Overexpression of p38IP and p38IP-N Rescues the Defects of p38IP-depleted Cells—To confirm whether the mitotic defects of p38IP-depleted cells directly resulted from p38IP disruption, we transfected p38IP, p38IP-N, and p38IP-C deletion mutants back into shp38IP cells. Indeed, overexpression of p38IP or p38IP-N dramatically or largely attenuated the accumulation of cells in G_2/M, respectively; however, p38IP-C did not effectively rescue the abnormal G_2/M accumulation of shp38IP cells, although it showed very high expression (Fig. 9*A*). In

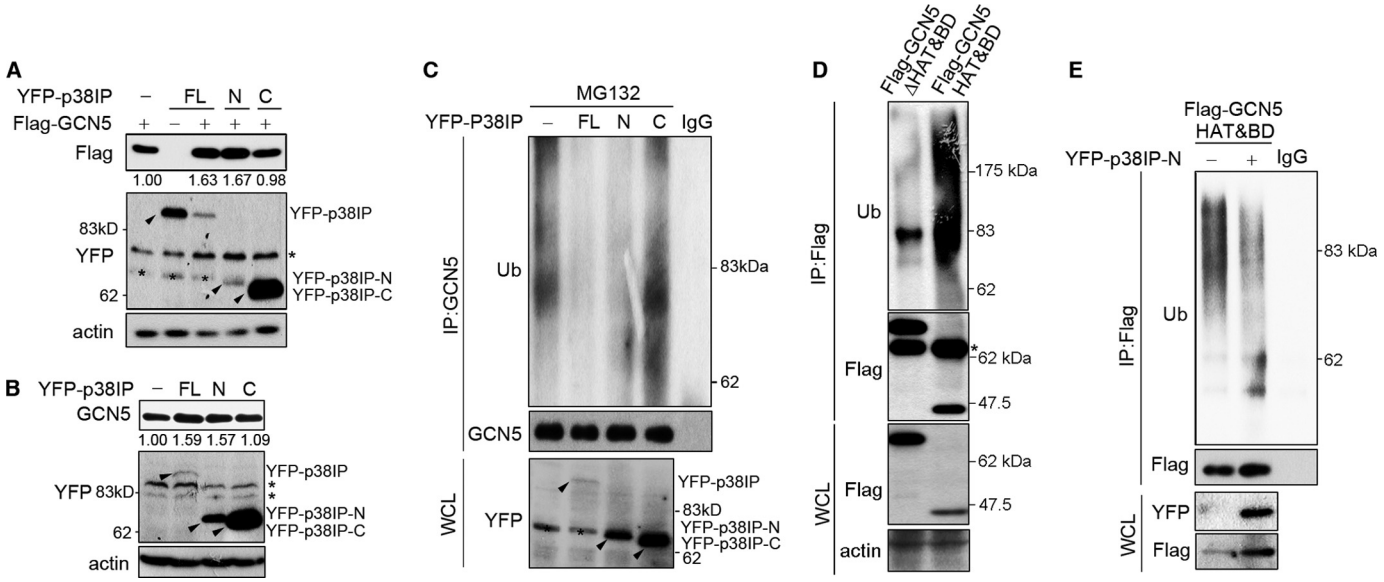

FIGURE 7. **The N terminus of p38IP is responsible for GCN5 stability.** *A* and *B*, overexpression of p38IP and p38IP-N but not p38IP-C increased GCN5 protein level. Cells were transfected with p38IP deletion mutants with or without FLAG-GCN5 as indicated, and Western blot analyses of exogenous GCN5 in 293T (*A*) and endogenous GCN5 in HeLa (*B*) cells were performed using the indicated antibodies. * indicates a nonspecific band. *FL*, full length; *N*, p38IP N terminus; *C*, p38IP C terminus. *C*, N terminus of p38IP inhibited GCN5 ubiquitination. 293T cells were transfected with YFP-p38IP, YFP-p38IP-N, and YFP-p38IP-C as indicated and then incubated with MG132. WCL were immunoprecipitated (*IP*) with anti-GCN5 antibody followed by immunoblotting with ubiquitin (*Ub*) and GCN5 antibodies. * indicates a nonspecific band. *D*, GCN5HAT&BD was heavily ubiquitinated. Whole cell extracts from 293T cells co-expressing the indicated constructs were immunoprecipitated with anti-FLAG antibody followed by immunoblotting with anti-ubiquitin and anti-FLAG antibodies. WCL were blotted as indicated. *E*, p38IP-N greatly suppressed ubiquitination of FLAG-GCN5HAT&BD. WCL from 293T cells co-expressing the indicated constructs were immunoprecipitated with anti-FLAG antibody followed by blotting with anti-ubiquitin and anti-FLAG antibodies. WCL were blotted as indicated.

shp38IP cells, re-expression of full-length p38IP markedly recovered GCN5 protein level and significantly reversed cyclin A/B accumulation and α-tubulin hypoacetylation; re-expression of p38IP-N could also obviously rescue GCN5 stability and acetylation of α-tubulin, but it did not affect the abundance of cyclin A and B as full-length p38IP did (Fig. 9*B*). Moreover, both p38IP and p38IP-N could effectively reshape defective spindles induced by p38IP depletion (Fig. 9*C*), and the extended vertical distance between two centrosomes was greatly alleviated in the presence of full-length p38IP or p38IP-N (Fig. 9*D*). Altogether, our data suggest that p38IP regulates G_2/M progression mainly through its N terminus, which maintains GCN5 stability and in turn α-tubulin acetylation. The model of the role of p38IP in the regulation of cell cycle G_2/M progression is shown in Fig. 9*E*.

DISCUSSION

In this study, we have uncovered an essential role and mechanism of p38IP in regulating mammalian cell G_2/M progression. We have demonstrated that by interacting with GCN5, p38IP blocks the proteasome-dependent degradation of GCN5, likely via nuclear sequestration of GCN5, and thus stabilizes GCN5 protein, thereby promoting the acetylation of α-tubulin, leading to stable mitotic spindle formation and maintaining proper G_2/M progression.

In this study, knockdown of p38IP impeded cell proliferation, which was consistent with the phenotype observed in ySpt20$^{-/-}$ yeast strains (34). Further evidence showed that this impediment in cell proliferation was caused by p38IP knockdown-induced G_2/M cell cycle arrest, which appeared to contradict previous reports that p38IP did not participate in cell cycle regulation (20). This contradiction indeed resulted from the different methods and criteria employed. Our conclusion that p38IP is required for cell cycle procession is drawn from the analysis of the percentage of cells with 2N and 4N DNA content, which is a generally accepted standard, whereas Orpinell *et al.* (20) determined that p38IP was not involved in mitosis because more than two centrosomes were not observed after p38IP depletion.

In the exploration of how p38IP affects the cell cycle, we proved that p38IP depletion-induced degradation of GCN5 is the key determinant. It is known that human p38IP as well as ySpt20 is required for the integrity of the SAGA complex (13, 16); however, the detailed mechanism remains unknown. Our work shows that p38IP stabilizes GCN5 by binding to and in turn inhibiting the ubiquitination of GCN5 HAT domain and bromodomain, which may result from p38IP blocking the association between GCN5 and its ubiquitin E3 ligase. Next, we find that ectopic expression of p38IP increases nuclear distribution of GCN5 HAT&BD, whereas depletion of p38IP increased the cytosolic/nuclear GCN5 ratio, indicating a positive correlation between GCN5 ubiquitination and cytosolic localization. Therefore, we may propose that p38IP segregates GCN5 into the nucleus, away from its potential cytosolic E3 ligase. A Cullin4-RING E3[5] ubiquitin ligase complex (CRL4) containing

[5] Cullin4-RING E3 ubiquitin ligase (CRL4) is a member of Cullin-RING E3 ligase family that is characterized by its enzymatic core that contains a Cullin family member and a RING protein. The Cullin family is a family of hydrophobic proteins providing a scaffold for E3 ubiquitin ligases, and a RING (really interesting new gene) finger protein is a specialized type of zinc finger protein that mediates the transfer the ubiquitin to substrates (41).

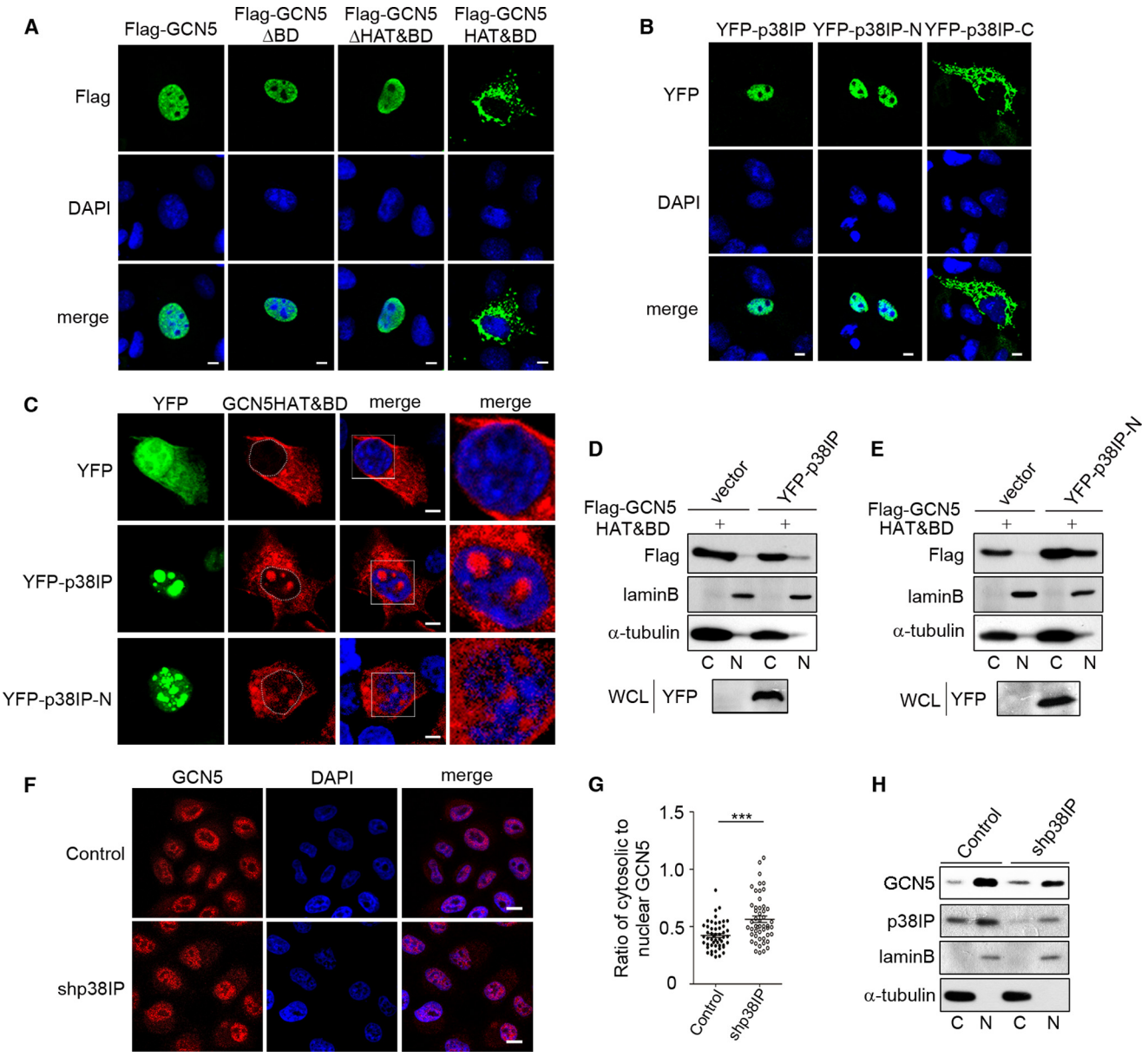

FIGURE 8. **p38IP stabilizes GCN5 by promoting GCN5 nuclear translocation.** *A*, cellular localizations of GCN5 full-length and its truncated mutants. The indicated constructs were overexpressed in 293T cells and visualized by staining with anti-FLAG antibody (*green*). DNA was stained with DAPI (*blue*) (*scale bar*: 5 μm). *B*, cellular localization of YFP-p38IP and its truncated mutants in 293T cells. DNA was stained with DAPI (*blue*) (*scale bar*: 5 μm). *C*, immunofluorescence of FLAG-GCN5HAT&BD (*red*) in 293T cells transfected with empty vector (*green*), p38IP (*green*), or p38IP-N (*green*). DNA was stained with DAPI (*blue*) (*scale bar*: 5 μm). *D* and *E*, cytosolic (*C*) and nuclear (*N*) protein extracts of 293T cells co-expressing FLAG-GCN5HAT&BD together with p38IP (*D*) or with p38IP-N (*E*) were subjected to Western blot with the indicated antibodies. *C*, cytosolic extract; *N*, nuclear extract. α-Tubulin and lamin B were used as the cytosolic marker and nuclear marker, respectively. *F* and *G*, p38IP depletion increased GCN5 cytosolic localization. Immunofluorescence was performed in HeLa cells for GCN5 (*red*). DNA was visualized by DAPI (*blue*) (*scale bar*: 10 μm). *G*, quantification of the ratio of cytosolic to nuclear GCN5 shown in *F* ($n = 50$ cells from three independent experiments, mean $\pm$ S.E., ***, $p < 0.001$). *H*, cells were treated with 10 μM MG132 for 4 h, and then cytosolic and nuclear protein extracts were prepared and subjected to immunoblotting with the indicated antibodies. *C*: cytosolic extract; *N*: nuclear extract. α-Tubulin and lamin B were used as the cytosolic marker and nuclear marker, respectively.

Cdt2[6] as the substrate recognition adaptor has been suggested to be the E3 of GCN5 (33), yet we cannot detect the association between Cdt2 and GCN5 in this study. It has been demonstrated that $CRL4^{Cdt2}$ degrades GCN5 in the nucleus (33); nevertheless, our data suggest that the degradation of GCN5 may occur in the cytosol, and thus, the E3 ligase responsible for p38IP depletion-induced degradation of GCN5 could be a ligase other than $CRL4^{Cdt2}$.

Intriguingly, knockdown of p38IP or GCN5 blocked the acetylation of α-tubulin, resulting in weak spindle formation. This finding was consistent with a previous study indicating that Myc-nick induced α-tubulin acetylation by recruiting GCN5 to microtubules during muscle cell differentiation (29). Unexpectedly, this finding seems to conflict with the conclusion that the ATAC complex controls mitotic progression by

[6] Cdt2 is Cdc10 (cell division control protein 10)-dependent transcript 2, the substrate recognition subunit of the CRL4Cdt2 ubiquitin ligase.

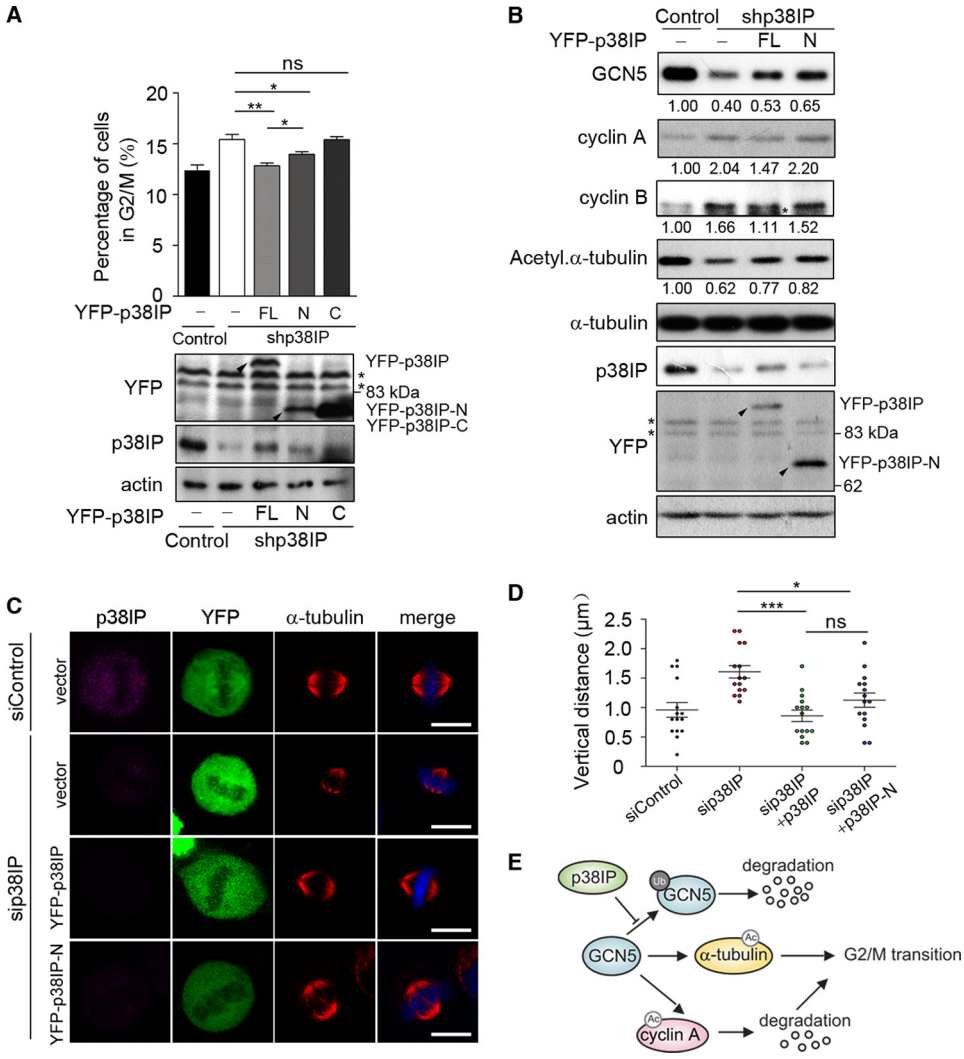

FIGURE 9. **Overexpression of p38IP and p38IP-N rescues the defects caused by p38IP knockdown.** *A*, overexpression of p38IP and p38IP-N in deficient cell lines alleviated the G_2/M accumulation. YFP-p38IP, YFP-p38IP-N, YFP-p38IP-C, and YFP vector were separately transfected into shp38IP HeLa cells. Cell cycle distribution was analyzed by propidium iodide staining and flow cytometry 24 h after transfection. Expression of transfected proteins was assessed by blotting as indicated. (mean ± S.E., $n = 3$, *,**, $p < 0.05$, *ns* indicates no significant difference). * indicates a nonspecific band. *B*, shp38IP cells were transfected with full-length p38IP, P38IP-N or YFP vector. 24 h after transfection, cells were analyzed by Western blot with the indicated antibodies. * indicates a nonspecific band. *C*, HeLa cells were co-transfected with siRNAs and YFP empty vector, YFP-p38IP, or YFP-p38IP-N as indicated. 24 h after transfection, cells were synchronized by thymidine block and collected 10 h after release. Mitotic spindle was visualized by staining with α-tubulin (*red*), and DNA was stained with DAPI (*blue*) (*scale bar*: 10 μm). *D*, quantification of the average vertical distance between two centrosomes in metaphase cells transfected with siRNAs and constructs as indicated and then treated as in *C* ($n = 15$ cells, mean ± S.E., ***, $p < 0.001$,*, $p < 0.05$, *ns* indicates no significant difference), *z* sections were taken at 0.2-μm increments. The data shown are representative of three independent experiments. *E*, the model for the function of p38IP in the regulation of cell cycle progression by inhibiting ubiquitination-induced degradation of GCN5.

GCN5 indirectly down-regulating the acetylation of α-tubulin (20). This contradiction may be because the specific subunits of SAGA or the ATAC complex can modulate GCN5 enzymatic activity and specificity. Together, our results and those of Orpinell *et al.* (20) on microtubule stability indicate that the hyperacetylation of α-tubulin caused by ATAC complex deficiency, which marked more static microtubules, might resist the pulling and pushing forces on the spindle and thus block the cells at the M/G_1 transition. By contrast, the hypoacetylation of α-tubulin caused by SAGA complex deficiency, which is marked by decreased microtubule stability, might interfere with mature mitotic spindle formation and thus arrest the cells at the G_2/M phase (35–38). The instability of microtubule proteins induced by p38IP depletion may also explain why p38IP-depleted cells have a smaller size because microtubules are required for cell shape and unstable microtubules may not be strong enough to support cells with a normal size.

Because α-tubulin localizes to the cytosol and GCN5 primarily localizes to the nucleus, how can GCN5 acetylate α-tubulin? From our results in Fig. 8, *F–H*, we can see that there is a small amount of GCN5 in the cytosol. GCN5 also constitutively associates with α-tubulin, and the association peaked at G_2/M (Fig. 5, *E* and *G*), which coincided with nuclear envelope breakdown at the G_2/M transition. This association resulted in the constitutive acetylation of α-tubulin throughout the cell cycle, with the strongest acetylation at the G_2/M transition (Fig. 3*G*), facilitating not only mitotic spindle assembly but also cell shape maintenance.

Of note, the p38IP N terminus could rescue p38IP depletion-induced α-tubulin hypoacetylation as efficiently as full-length

p38IP but could not rescue the cyclin A and B defects (Fig. 9*B*). Meanwhile, knockdown or ectopic expression of GCN5 leads to the respective accumulation or decrease of cyclin A (Fig. 5, *A* and *B*). These results suggest that p38IP-C terminus is required for cooperation with GCN5 in the regulation of cyclins. Here, a question remains. As GCN5 by rescued p38IP-N can restore the acetylation of α-tubulin, why can it not release the accumulation of cyclins that may result from hypoacetylation? We propose that this might be attributed to the association affinity of GCN5 with α-tubulin or cyclin A; depletion of p38IP does not affect α-tubulin binding to GCN5 (Fig. 5*E*), whereas recruitment of cyclin A to GCN5 may require the p38IP C terminus. Alternatively, the cyclin defects induced by p38IP depletion could be caused by an independent function of the p38IP C terminus, which is essential for association with p38 (15).

Altogether, this is the first demonstration of the essential role of p38IP in G_2/M progression and reveals the mechanism by which p38IP maintains SAGA complex integrity by stabilizing GCN5. The similar but distinct functions of the SAGA and ATAC complexes in cell cycle regulation suggest the decisive role of the specific subunits in the SAGA (such as p38IP) or ATAC complexes and the complexity and delicacy of the GCN5-containing complex to adapt to distinct physiological requirements. This study sheds new light on understanding the critical value of p38IP in the regulation of the cell cycle and the GCN5-SAGA complex.

REFERENCES

1. Lucchini, G., Hinnebusch, A. G., Chen, C., and Fink, G. R. (1984) Positive regulatory interactions of the HIS4 gene of *Saccharomyces cerevisiae*. *Mol. Cell. Biol.* **4,** 1326–1333
2. Hinnebusch, A. G., and Fink, G. R. (1983) Positive regulation in the general amino acid control of *Saccharomyces cerevisiae*. *Proc. Natl. Acad. Sci. U.S.A.* **80,** 5374–5378
3. Brownell, J. E., Zhou, J., Ranalli, T., Kobayashi, R., Edmondson, D. G., Roth, S. Y., and Allis, C. D. (1996) Tetrahymena histone acetyltransferase A: a homolog to yeast Gcn5p linking histone acetylation to gene activation. *Cell* **84,** 843–851
4. Georgakopoulos, T., and Thireos, G. (1992) Two distinct yeast transcriptional activators require the function of the GCN5 protein to promote normal levels of transcription. *EMBO J.* **11,** 4145–4152
5. Wang, L., Mizzen, C., Ying, C., Candau, R., Barlev, N., Brownell, J., Allis, C. D., and Berger, S. L. (1997) Histone acetyltransferase activity is conserved between yeast and human GCN5 and is required for complementation of growth and transcriptional activation. *Mol. Cell. Biol.* **17,** 519–527
6. Candau, R., Moore, P. A., Wang, L., Barlev, N., Ying, C. Y., Rosen, C. A., and Berger, S. L. (1996) Identification of human proteins functionally conserved with the yeast putative adaptors ADA2 and GCN5. *Mol. Cell. Biol.* **16,** 593–602
7. Zhang, W., Bone, J. R., Edmondson, D. G., Turner, B. M., and Roth, S. Y. (1998) Essential and redundant functions of histone acetylation revealed by mutation of target lysines and loss of the Gcn5p acetyltransferase. *EMBO J.* **17,** 3155–3167
8. Vernarecci, S., Ornaghi, P., Bâgu, A., Cundari, E., Ballario, P., and Filetici, P. (2008) Gcn5p plays an important role in centromere kinetochore function in budding yeast. *Mol. Cell. Biol.* **28,** 988–996
9. Xu, W., Edmondson, D. G., Evrard, Y. A., Wakamiya, M., Behringer, R. R., and Roth, S. Y. (2000) Loss of Gcn5l2 leads to increased apoptosis and mesodermal defects during mouse development. *Nat. Genet.* **26,** 229–232
10. Lin, W., Srajer, G., Evrard, Y. A., Phan, H. M., Furuta, Y., and Dent, S. Y. (2007) Developmental potential of $Gcn5^{-/-}$ embryonic stem cells *in vivo* and *in vitro*. *Dev. Dyn.* **236,** 1547–1557
11. Paolinelli, R., Mendoza-Maldonado, R., Cereseto, A., and Giacca, M. (2009) Acetylation by GCN5 regulates CDC6 phosphorylation in the S phase of the cell cycle. *Nat. Struct. Mol. Biol.* **16,** 412–420
12. Marcus, G. A., Silverman, N., Berger, S. L., Horiuchi, J., and Guarente, L. (1994) Functional similarity and physical association between GCN5 and ADA2: putative transcriptional adaptors. *EMBO J.* **13,** 4807–4815
13. Grant, P. A., Duggan, L., Côté, J., Roberts, S. M., Brownell, J. E., Candau, R., Ohba, R., Owen-Hughes, T., Allis, C. D., Winston, F., Berger, S. L., and Workman, J. L. (1997) Yeast Gcn5 functions in two multisubunit complexes to acetylate nucleosomal histones: characterization of an Ada complex and the SAGA (Spt/Ada) complex. *Genes Dev.* **11,** 1640–1650
14. Spedale, G., Timmers, H. T., and Pijnappel, W. W. (2012) ATAC-king the complexity of SAGA during evolution. *Genes Dev.* **26,** 527–541
15. Zohn, I. E., Li, Y., Skolnik, E. Y., Anderson, K. V., Han, J., and Niswander, L. (2006) p38 and a p38-interacting protein are critical for downregulation of E-cadherin during mouse gastrulation. *Cell* **125,** 957–969
16. Nagy, Z., Riss, A., Romier, C., le Guezennec, X., Dongre, A. R., Orpinell, M., Han, J., Stunnenberg, H., and Tora, L. (2009) The human SPT20-containing SAGA complex plays a direct role in the regulation of endoplasmic reticulum stress-induced genes. *Mol. Cell. Biol.* **29,** 1649–1660
17. Wang, Y. L., Faiola, F., Xu, M., Pan, S., and Martinez, E. (2008) Human ATAC Is a GCN5/PCAF-containing acetylase complex with a novel NC2-like histone fold module that interacts with the TATA-binding protein. *J. Biol. Chem.* **283,** 33808–33815
18. Welihinda, A. A., Tirasophon, W., Green, S. R., and Kaufman, R. J. (1997) Gene induction in response to unfolded protein in the endoplasmic reticulum is mediated through Ire1p kinase interaction with a transcriptional coactivator complex containing Ada5p. *Proc. Natl. Acad. Sci. U.S.A.* **94,** 4289–4294
19. Webber, J. L., and Tooze, S. A. (2010) Coordinated regulation of autophagy by p38α MAPK through mAtg9 and p38IP. *EMBO J.* **29,** 27–40
20. Orpinell, M., Fournier, M., Riss, A., Nagy, Z., Krebs, A. R., Frontini, M., and Tora, L. (2010) The ATAC acetyl transferase complex controls mitotic progression by targeting non-histone substrates. *EMBO J.* **29,** 2381–2394
21. den Elzen, N., Buttery, C. V., Maddugoda, M. P., Ren, G., and Yap, A. S. (2009) Cadherin adhesion receptors orient the mitotic spindle during symmetric cell division in mammalian epithelia. *Mol. Biol. Cell* **20,** 3740–3750
22. Samora, C. P., Mogessie, B., Conway, L., Ross, J. L., Straube, A., and McAinsh, A. D. (2011) MAP4 and CLASP1 operate as a safety mechanism to maintain a stable spindle position in mitosis. *Nat. Cell Biol.* **13,** 1040–1050
23. Dumont, S., and Mitchison, T. J. (2009) Compression regulates mitotic spindle length by a mechanochemical switch at the poles. *Curr. Biol.* **19,** 1086–1095
24. Gavet, O., and Pines, J. (2010) Progressive activation of CyclinB1-Cdk1 coordinates entry to mitosis. *Dev. Cell* **18,** 533–543
25. Gong, D., Pomerening, J. R., Myers, J. W., Gustavsson, C., Jones, J. T., Hahn, A. T., Meyer, T., and Ferrell, J. E., Jr. (2007) Cyclin A2 regulates nuclear-envelope breakdown and the nuclear accumulation of cyclin B1. *Curr. Biol.* **17,** 85–91
26. den Elzen, N., and Pines, J. (2001) Cyclin a is destroyed in prometaphase and can delay chromosome alignment and anaphase. *J. Cell Biol.* **153,** 121–136
27. Wickström, S. A., Masoumi, K. C., Khochbin, S., Fässler, R., and Massoumi, R. (2010) CYLD negatively regulates cell-cycle progression by inactivating HDAC6 and increasing the levels of acetylated tubulin. *EMBO J.* **29,** 131–144
28. Perdiz, D., Mackeh, R., Poüs, C., and Baillet, A. (2011) The ins and outs of tubulin acetylation: more than just a post-translational modification? *Cell. Signal.* **23,** 763–771
29. Conacci-Sorrell, M., Ngouenet, C., and Eisenman, R. N. (2010) Myc-nick: a cytoplasmic cleavage product of Myc that promotes α-tubulin acetylation and cell differentiation. *Cell* **142,** 480–493
30. Piperno, G., LeDizet, M., and Chang, X. J. (1987) Microtubules containing acetylated α-tubulin in mammalian cells in culture. *J. Cell Biol.* **104,** 289–302
31. Blagosklonny, M. V., Robey, R., Sackett, D. L., Du, L., Traganos, F., Dar-

zynkiewicz, Z., Fojo, T., and Bates, S. E. (2002) Histone deacetylase inhibitors all induce p21 but differentially cause tubulin acetylation, mitotic arrest, and cytotoxicity. *Mol. Cancer Ther.* **1,** 937–941
32. Barlev, N. A., Poltoratsky, V., Owen-Hughes, T., Ying, C., Liu, L., Workman, J. L., and Berger, S. L. (1998) Repression of GCN5 histone acetyltransferase activity via bromodomain-mediated binding and phosphorylation by the Ku-DNA-dependent protein kinase complex. *Mol. Cell. Biol.* **18,** 1349–1358
33. Li, Y., Jaramillo-Lambert, A., Hao, J., Yang, Y., and Zhu, W. (2011) The stability of histone acetyltransferase general control non-derepressible (Gcn) 5 is regulated by Cullin4-RING E3 ubiquitin ligase. *J. Biol. Chem.* **286,** 41344–41352
34. Roberts, S. M., and Winston, F. (1996) SPT20/ADA5 encodes a novel protein functionally related to the TATA-binding protein and important for transcription in *Saccharomyces cerevisiae*. *Mol. Cell. Biol.* **16,** 3206–3213
35. Steuer, E. R., Wordeman, L., Schroer, T. A., and Sheetz, M. P. (1990) Localization of cytoplasmic dynein to mitotic spindles and kinetochores. *Nature* **345,** 266–268
36. Vaisberg, E. A., Koonce, M. P., and McIntosh, J. R. (1993) Cytoplasmic dynein plays a role in mammalian mitotic spindle formation. *J. Cell Biol.* **123,** 849–858
37. Reed, N. A., Cai, D., Blasius, T. L., Jih, G. T., Meyhofer, E., Gaertig, J., and Verhey, K. J. (2006) Microtubule acetylation promotes kinesin-1 binding and transport. *Curr. Biol.* **16,** 2166–2172
38. Dompierre, J. P., Godin, J. D., Charrin, B. C., Cordelières, F. P., King, S. J., Humbert, S., and Saudou, F. (2007) Histone deacetylase 6 inhibition compensates for the transport deficit in Huntington's disease by increasing tubulin acetylation. *J. Neurosci.* **27,** 3571–3583
39. Timmers, H. T., and Tora, L. (2005) SAGA unveiled. *Trends Biochem. Sci.* **30,** 7–10
40. Zeng, L., and Zhou, M. M. (2002) Bromodomain: an acetyl-lysine binding domain. *FEBS Lett.* **513,** 124–128
41. Petroski, M. D., and Deshaies, R. J. (2005) Function and regulation of cullin-RING ubiquitin ligases. *Nat. Rev Mol. Cell Biol.* **6,** 9–20